Chapter 5

Light Higgs Physics at the Tevatron

5.1 Introduction

One of the primary goals of present and future colliders is to discover the mechanism responsible for the spontaneous symmetry breaking of the $SU(2)_L \times U(1)_Y$ electroweak interaction. The simplest model for this mechanism is the standard Higgs model, based on a doublet of fundamental scalar fields. This model predicts the existence of a new particle, the Higgs boson, of unknown mass, but with fixed couplings to other particles. The search for the Higgs boson represents a benchmark in our search for the mechanism of electroweak symmetry breaking.

The current lower bound on the Higgs mass is 64.5 GeV from LEP. In the near future, LEP II will extend the search to higher masses via $e^+e^- \to ZH$. The reach in Higgs mass depends on the machine energy, and is roughly $m_H < \sqrt{s} - M_Z - (5-10)$ GeV. The current plan is for LEP II to achieve $\sqrt{s} = 184$ GeV in 1996, which would cover up to $m_H = 85$ GeV. In 1999, the energy will be further increased to $\sqrt{s} = 192$ GeV, which will allow coverage up to $m_H \approx 95$ GeV.

Much higher Higgs masses will be explored by the CERN Large Hadron Collider (LHC), beginning in 2004 at $\sqrt{s} = 10$ TeV and increasing to $\sqrt{s} = 14$ TeV in 2008. For example, the process $gg \to H \to ZZ \to \ell^+\ell^-\ell^+\ell^-$ will cover from $m_H \approx 130 - 700$ GeV at full energy and luminosity [1, 2].

Ironically, the light intermediate-mass region, $m_H \approx 80 - 130$ GeV, which is the favored region for a SUSY Higgs boson, is the most difficult at the LHC. The CMS detector intends to cover this region with the rare decay $H \to \gamma\gamma$ [1]. The ATLAS detector covers down to $m_H \approx 110$ GeV with this mode, and requires 500 fb^{-1} to cover down to $m_H \approx 80$ GeV [2].

The dominant decay mode of the Higgs boson in this mass range is $H \to b\bar{b}$; the branching ratio is about 80%. There does not exist any established method to detect the Higgs in this decay mode at the LHC (see the section on the LHC for more details). It has been suggested that the process $q\bar{q} \to WH$, followed by $H \to b\bar{b}$ and leptonic decay of the W boson, could be used at the Tevatron to discover the light intermediate-mass Higgs boson [3, 4, 5]. This is discussed in the next section. This signal may be more difficult to detect at the LHC due to the very large top-quark background.

The most useful subleading decay mode of the Higgs boson in the light intermediate-mass range is $H \to \tau^+\tau^-$, with a branching ratio of about 8% [9]. It has been suggested that the process $q\bar{q} \to (W,Z)H$, followed by $H \to \tau^+\tau^-$ and $W,Z \to jj$ (j denotes a jet) could be used at the Tevatron for Higgs masses above the Z mass, roughly $m_H > 110$ GeV [4]. This is discussed in the third section. This process is hopeless at the LHC due to the enormous $(Z \to \tau^+\tau^-)jj$ background.

Precision electroweak data weakly favor a light Higgs boson, with the best fit from LEP and SLC data centered on $m_H \approx 100$ GeV. It is vital that we not leave the intermediate-mass Higgs window open, and the Tevatron can potentially play a crucial role in closing this window.

The standard Higgs model has a number of unappealing features, such as the *ad hoc* introduction of fundamental scalar fields with special interactions, and difficulties with naturally producing electroweak symmetry breaking at the weak scale rather than some much higher energy scale. A supersymmetric model ameliorates many of these problems. The minimal supersymmetric standard model requires two Higgs doublets, yielding a spectrum of Higgs bosons: two neutral scalars, h and H; a neutral pseudoscalar, A; and a charged pair, $H^\pm$. There is an upper bound on the mass of the lightest scalar, h, which depends on the top quark and top squark masses. For $m_t = 175$ GeV and $m_{\tilde{t}} < 1$ TeV, this bound is $m_h < 125$ GeV. The couplings of this Higgs boson to ordinary particles are usually very close to those of the standard Higgs boson. However, the coupling to bottom quarks (and τ leptons) is sometimes enhanced, which suppresses the rare decay to two photons. Thus there is a region of SUSY parameter space in which the h is invisible at the LHC. In fact, throughout most of this region, none of the SUSY Higgs particles are visible. Thus the $h \to b\bar{b}$ and $h \to \tau^+\tau^-$ modes at the Tevatron could be crucial for exploring the Higgs sector of the minimal SUSY model.

5.2 $q\bar{q} \to WH$ with $H \to b\bar{b}$

5.2.1 Introduction and Selection Cuts

The associated production of a Higgs boson and a W or Z boson, with the Higgs decaying to $b\bar{b}$ and the W or Z decaying leptonically, is a possible way to detect the Higgs in the mass range 60-130 GeV. As an example, the total Standard Model cross section for WH (Higgs mass 80 GeV) at $\sqrt{s} = 2\,TeV$ is $\approx 500fb$, and coupled with the 2/9 branching ratio of the W into electrons or muons, means that with small backgrounds one could consider such searches with integrated luminosities of less than $1fb^{-1}$. The question then becomes: What are the backgrounds? The Higgs decays give rise to 2 jets, thus we will start with the basic W+2 jet backgrounds. This will lead to the issue of b tagging, and the physics backgrounds that include a W and one or more b quarks. After considering the signal and all the backgrounds, we will observe the importance of dijet mass resolution, which appears to be the "make or break" issue in finding the Higgs in the W+H mode. We will compare the prospects for the same measurements at the LHC. We will also find that observing a Higgs with mass of 100-130 GeV is more complicated than 60-100 GeV. The 100-130 GeV Higgs search depends

critically on statistics and uncertain (at present) top backgrounds. We will discuss in some detail how much luminosity is needed to reduce the statistical *and* systematic uncertainties to an acceptable level to find the 100-130 GeV Higgs.

The default cuts in this note are those in ref [3], and are briefly summarized as follows: a) both b jets $p_t > 15\ GeV$ and $|y| < 2.0$, b) typical W cuts on leptons + missing E_t, and c) no extra jets with $p_t > 30\ GeV$ (or two extra jets above 15 GeV) and no extra leptons with $p_t > 20\ GeV$ to reduce top backgrounds. Jets were clustered with the CDF cone algorithm, with a 0.7 cone-size. By default we will make the b jet energy corrections CDF uses in the top search for vertex-tagged jets.

5.2.2 $W + 2$ Jet Backgrounds to WH, b tagging

A light, SM Higgs will decay to $b\bar{b}$ 82% of the time, $\tau\bar{\tau}$ 9%, $c\bar{c}$ 8%, and $s\bar{s}$ 1%. Without further information, each decay mode gives rise to two jets. We thus begin with the backgrounds from a leptonic W decay, and two jets. We will measure the rate of this directly from present CDF data, then multiply the rate by a factor 1.3 to convert to $\sqrt{s} = 2$ TeV. Figure 5.1 shows this measurement, along with the expected distribution from an 80 GeV Higgs, produced in association with a W. All of the Higgs distributions in this note will be generated with PYTHIA + CDF's best calorimeter simulation, and the number of events normalized with the calculated NLO cross sections. This figure shows the W+2 jet backgrounds are a 1000 times larger than the expected signal, thus we will need significant additional handles. Since b tagging is now well established, and the $b\bar{b}$ decay mode is largest, it is natural to investigate b tagging first.

Tagging b quarks using displaced vertices and semi-leptonic decays is now well established. Tagging efficiencies on the other hand are often confusing. The most common number quoted is the efficiency for tagging at least one b quark in a $t\bar{t}$ event. This number depends on many different factors and is irrelevant for almost anything else. The number one wants for any other physics is how often a single b jet with a given energy will be tagged, if that jet is inside the relevant detector. Then the problem can be broken down into two parts, the fiducial acceptance for a certain jet from a certain process, and how often that jet is tagged. For the WH process in Run II and beyond it is even simpler. Both b jets have $|y| < 2.0$ a large fraction of the time, and the present upgrades of CDF/D0 are expected to have b tagging capabilities within this region. Thus the problem reduces to the tagging efficiency versus b jet energy, and this is shown in figure 5.2 for the present CDF detector if the b jet is in the fiducial region of the SVX. The efficiency at high energies is above 50%, and falls off at lower energies due to the necessary cuts on track p_t. The present probability for a non-heavy-flavor jet faking a b tag is $\approx 0.5\%$. The 50% efficiency and 0.5% fake rate are only estimates of course for Run II, but some factors such as improved silicon or pixel detectors will make these better, and some factors such as multiple interactions will make them worse. And these estimates do not include soft lepton tagging of b quarks. We will use 50%/0.5% as our best estimate at this time.

Once we have an estimate of b tagging potential, the issue is whether to use single or double b tagging. With single b tagging, the signal efficiency is 50%, and S/B improvement is 100, with double tagging the signal efficiency is 25%, and S/B improvement 10000. Figure 5.3

shows the resulting signal and background distributions for the two cases, only considering the W+2 jet fake backgrounds. We conclude that the W+2 jet backgrounds are too large to use single b tagging, and double tagging with the present algorithm is certainly sufficient, but it appears there is room for a "loose" double tag method that would improve the signal efficiency. We will not pursue this further, and will use double b tagging with the 50%/0.5% estimates mentioned earlier. Other physics backgrounds that include two b quarks are not reduced by b tagging, and these are considered next.

5.2.3 Backgrounds to WH containing heavy quarks

There are six other notable backgrounds to the WH process, each containing two heavy quarks already. They are the $Wb\bar{b}$ process, the WZ process with $Z \to b\bar{b}$, $t\bar{t}$, $W^* \to tb$ (offshell W), W-gluon fusion (t+q+b final state), and $Wc\bar{c}$ with the charm faking a b quark. We will state briefly what we have used to estimate each of these backgrounds.

The largest background to the WH process is $Wb\bar{b}$ production, and for this we use the matrix element calculation of Mangano, interfaced with the HERWIG shower monte carlo and the CDF calorimeter simulation. Figure 5.4 shows four kinematic distributions of this background, compared to the WH signal. This calculation is already being checked with W+tagged jet data, the background for the top quark. The backgrounds to the top search are mostly W+heavy quark production, thus the agreement with data in the W+1 jet and W+2 jet bins, where the top contribution is small, is a test already of the Mangano calculation. In addition, fits to $c\tau$ in these bins are being used to separate the $W + b\bar{b}$ and $W + c\bar{c}$ contributions. For the $W + c\bar{c}$ contribution to the Higgs, we have simply scaled down $W + b\bar{b}$ by 1/10, due to the calculated equal production cross section(by two groups), and the tagging efficiency which is 1/3 of the b tagging efficiency..

The WZ process, with $Z \to b\bar{b}$, is estimated with PYTHIA + CDF calorimeter simulation, then the cross section is normalized to the calculated NLO cross section of Ohnemus. As the process is initiated by $q\bar{q}$, these cross sections should be reliable. In addition, this background has the feature that with a few fb^{-1} of data, one can use the clean all-leptonic decay channels to normalize the $b\bar{b}$ decay mode. Figure 5.5 shows four kinematic distributions of this background, compared to the WH signal.

We have used the HERWIG $t\bar{t}$ generator + CDF calorimeter simulation, with a 6200fb total cross section to model this background. As with $W + b\bar{b}$ and WZ, with a few fb^{-1} of data we should have enough $t\bar{t}$ events to understand them well. One complication from this background are "dilepton" events where both Ws decay leptonically, and one of the leptons is not detected. This part of the $t\bar{t}$ background is very detector and analysis specific, thus is hard to estimate. Since the $t\bar{t}$ backgrounds are small at the Tevatron, we can safely ignore this contribution at this time. The same is true of τ+jet backgrounds. Figure 5.6 shows four kinematic distributions of this background, compared to the WH signal.

We have used the PYTHIA W^* generator + CDF calorimeter simulation, with a total cross section of 594fb, to model this background. Figure 5.7 shows four kinematic distributions of this background, compared to the WH signal. And finally we used HERWIG + simulation to model the W-gluon fusion(tqb) background with a total cross section of 2360fb. Figure 5.8 shows four kinematic distributions of this background, compared to the WH sig-

nal. These two backgrounds are small at the Tevatron at lower masses, but nevertheless are significant for Higgs masses 100-130 GeV. They are an experimental challenge in their own right, as they mix with each other, and with the much larger $t\bar{t}$ events.

Figure 5.9 summarizes all the backgrounds to the WH process. One can see that $W + b\bar{b}$ dominates at low masses, with the top backgrounds becoming significant for masses above 100 GeV. In table 5.2.8 we have compared our results for each background, in the different signal regions, with the reference [3] results. Overall they are very close for the important backgrounds, while there are remaining discrepancies with the small top backgrounds. The increase in the $W + b\bar{b}$ backgrounds at the fully simulated jet level, compared to the parton level used in reference [3], we believe is due to lower energy b partons fluctuating to higher energy due to detector effects.

5.2.4 Signal+Background Distributions

We have two choices to make before showing signal+background distributions, 1) optimized or non-optimized cuts, and 2) optimized or non-optimized jet resolutions. Reference [7] describes fairly sophisticated cuts at the parton level which give a x4 better S/B ratio than the cuts in reference [3] which we are using. The optimized cuts come from the $b\bar{b}$ angles, the center-of-mass scattering angles, and the total invariant mass of the event. We have investigated some of these optimized cuts very briefly, and do see improvements in S/B. But one complication with trying to use optimized cuts is that they will certainly be mass dependent, and different for the Tevatron and LHC which we compare later. Thus without further investigation we will assume as a default that we can maintain a x2 improvement in S/B at the full simulation level, then show later the effect of removing this improvement completely in a worst case scenario. Likewise for jet resolutions, we will pick a resolution as a default that is better than we currently observe from the simulation, but which is reasonable to assume can be achieved with more study. We will give the details of the jet resolutions we are using in the next section.

Figure 5.10 shows the signal+background distributions for Higgs masses 60,80,100,120 GeV for 1 fb^{-1} of data, with our "nominal" jet resolutions and the x2 improvement in S/B. The solid lines are the signal+background, while the dashed line is the sum of all backgrounds. Clearly this is not enough data to see anything. With 5 fb^{-1} of data, one can see the signal begin to emerge at lower masses in figure 5.11. With 10 fb^{-1} of data, figure 5.12 shows the signals for masses below 120 GeV have become more pronounced, while the 120 GeV Higgs is still not clearly seen. The excess at 60 GeV is more than 9 standard deviations above background, 80 GeV is more than 7 sigma, and 100 GeV is 4.9 sigma. These numbers are all without systematic uncertainties, of course, but in this mass range the dominant backgrounds will be $W + b\bar{b}$ and WZ, which should be well-understood by this time. Figure 5.13 is a blowup of the higher mass plots. There is a small excess at 120 GeV, but with only a small number of events and uncertain single top backgrounds this will be more difficult. In a later section we will discuss how much luminosity will be needed to find a 120 GeV Higgs, and whether it is possible Z+H signals can be used to supplement the high mass search.

We now present three variations of the plot for 10 fb^{-1}, in order to illustrate the sen-

sitivity to jet resolutions and optimized cuts. Figure 5.14 is the same plot, except using the present jet resolutions the simulation is giving. The clear peaks in the previous plot are now smeared out. As mentioned earlier, we feel with more study the resolution can be improved to the level of our choice of "nominal" resolution, this is discussed in a later section. If one uses the jet resolution used in reference [3], which is more optimistic than our "nominal", one gets sharper peaks as displayed in figure 5.15. In fact the 120 GeV Higgs starts to become noticeable, albeit still low statistics. Finally, we display the same plots with the best jet resolution, but with the x2 improvement in cuts removed. This is shown in figure 5.16, and corresponds to repeating the reference [3] study but with a full simulation of all the backgrounds, while keeping the signal mass resolution constant. Clearly the effect of optimized cuts is also very important in the Higgs search.

5.2.5 Comparison with LHC

We will make a simple extrapolation of the Tevatron studies to estimate the capability of the LHC to make the WH measurements. We will simply repeat the Tevatron analysis, but increase the number of events by the ratio of cross sections as given by HERWIG or PYTHIA, 14 TeV/2 TeV. This is optimistic in favor of the LHC for 2 reasons, the signal efficiency due to the extra jet cut is reduced at the LHC since there is more initial state radiation. This was checked with PYTHIA and the reduction is not that large, from 92% efficiency at the Tevatron to 72% at the LHC. The second reason this is optimistic is that the details of the $t\bar{t}$ backgrounds become important at the LHC, for example the ignored dilepton top events may be a significant background at the LHC. Nevertheless, it is very instructive to simply repeat the same analysis, with the same monte carlo data, with different total cross sections. The cross section ratios used are: 1) WH 60 GeV = 7.0, WH 80 GeV = 7.68, WH 100 GeV = 8.53, WH 120 GeV = 9.54, 2) WZ = 9.2, 3) $W + b\bar{b}$ and $W + c\bar{c}$ = 6.24, 4) $t\bar{t}$ = 104, 5) W^* = 12, 6) tqb = 85, 7) W+2 jet = 13. Figure 5.17 shows all the backgrounds to the WH process at the LHC. Compared to the Tevatron, it is clear the top quark backgrounds become important at much lower masses, since the cross section ratios for those backgrounds are so large. Figure 5.18 shows the signal and background distributions for the LHC. A 60 GeV Higgs clearly stands out, since the main background there is still $W + b\bar{b}$, but 80-100 GeV masses appear more difficult to observe at the LHC than at the Tevatron due to the increased top backgrounds.

5.2.6 Dijet Mass Resolutions

As mentioned previously, the issue of jet energy resolution, or more accurately dijet mass resolution, is crucial to finding the Higgs in Run II. We have used three different mass resolutions, now we specify what those are: 1) The "best" resolution, used in reference [3], is $0.8/\sqrt{M}+0.03$, with the two terms added in quadrature. This gives a 7.5 GeV resolution at 80 GeV. 2) The "nominal" resolution, $1.0/\sqrt{M}+0.03$, with the two terms added linearly. This gives an 11.3 GeV resolution at 80 GeV. 3) The "worst" resolution, which is from the full simulation results without optimization, gives a resolution of 15.5 GeV at 80 GeV.

To investigate the source of the increase in resolution with the full simulation, we gen-

erated a sample of single W events, with the W decaying to 2 jets. When matching the daughter quark direction to the measured jet direction, there is a large peak near zero in delta-R, but also a well-known long tail expected from hard gluon radiation. If we separate the events into two classes, delta-R>0.2 and delta-R<0.2, we get two very different W mass distributions, the small delta-R peaked at 80 GeV with an 11 GeV RMS, while large delta-R peaked at 60 GeV and very broad. The combined distribution has an RMS of 15.5 GeV, shown in figure 5.19. The events with large delta-R have been checked and an extra jet does appear in the detector most of the time. Thus one large component of the dijet mass resolution is from physics, and does not depend on the detector. Clearly an intelligent algorithm needs to be developed to include these extra jets, whether with the cone algorithm or the Kt algorithm. Additional improvements in dijet mass resolution are possible by using charge tracks, shower maximum detectors for photons, etc. It clearly is crucial for this physics to improve the dijet mass resolution in all ways possible, whether by physics effects or detector effects.

One other concern is that we will optimize our jet resolutions, then lose it all due to multiple interactions. To investigate this we generated the 80 GeV signal events with 5 additional interactions (6 total), and 8 additional interactions (9 total). Figure 5.20 shows the mass resolution for the 6 interaction case, the mean has shifted but the width has not significantly increased. The same was true of the 9 interaction case. This is with a cone radius 0.7, with smaller cones one will be less sensitive, with larger cones or perhaps a Kt algorithm we will be more sensitive to pileup. And the extra interactions may harm any algorithm we devise to merge in soft extra jets. But with the basic algorithm used in this note, additional interactions do not seem to be a problem in mass resolution.

5.2.7 Masses above 100 GeV

It has been shown that the Higgs masses above 100 GeV are more difficult to observe than the lower masses. This is mostly due to the smaller cross sections, but also due to the top backgrounds that only contribute at larger masses. Here we will discuss briefly what it might take to observe a 120 GeV Higgs. This will include how much data it would take, using only the WH mode, as well as the possibility of using the Z+H mode, which do not have top backgrounds.

In figure 5.13 there is a closeup of the 120 GeV Higgs with 10 fb^{-1}. If one takes an objective mass range such as the Willenbrock range, without looking at the data fluctuations, then there is a 3.3σ statistical excess in this plot from 102-141 GeV. Namely 27 events on a background of 65. If one simply scales this up to get a 5σ excess, one needs $\approx 25 fb^{-1}$ of data. Then there are systematics. Of the 65 background events 19 are from top backgrounds. Thus assuming the other backgrounds are known well, one would have to have a total systematic on the combined top backgrounds of $\approx 25\%$ to get a 5σ excess. There will certainly be measurements of W^* and tqb production with 10 fb^{-1} or less, but not only will the cross sections need to measured independently, but how often they pass the tight Higgs analysis cuts needs to be estimated. We believe it likely that this can be done accurately with 25 fb^{-1}, but probably not with only 10 fb^{-1}. Thus from both the statistics and systematics of the analysis, it seems 25 fb^{-1} is necessary to measure a 120 GeV Higgs in the WH channel

alone.

If one is only trying to find the Higgs, rather than measuring the WH coupling alone, then perhaps Z+H modes could supplement the 120 GeV Higgs search and make it possible with only 5-10 fb^{-1}. The events with a Z decay to electrons and muons only add about 15% to the WH cross section, so this is not much help. The $Z \to \nu\bar{\nu} + H \to \tau\bar{\tau}$ mode has been investigated by D0 and does not look promising. The $Z \to \nu\bar{\nu} + H \to b\bar{b}$ mode offers another possibility. We have generated this mode with Pythia, and find the signal can be triggered on with 85% efficiency in CDF with the missing-Et trigger of 35 GeV. The question then becomes the backgrounds, which would be a useful study to pursue in detail in the future.

5.2.8 Conclusions for $q\bar{q} \to WH$ with $H \to b\bar{b}$

We have investigated the potential to observe the Higgs particle in the production mode $W + H \to \ l\nu + b\bar{b}$ at the Tevatron. We find that with 25 fb^{-1} this process will enable the observation of a Higgs boson up to $m_H \sim 120$ GeV/c^2.

With modest improvements to jet energy resolutions, a 60-100 GeV Higgs is observable with just 5-10 fb^{-1}. Physics effects appear to play an important role in the dijet mass resolutions, thus studies of jet clustering may be more important than detector resolutions. Discovering a 100-130 GeV Higgs in this mode alone, with only 5-10 fb^{-1}, will be more difficult because of low statistics and somewhat uncertain single top backgrounds, and argues for more luminosity. For any mass range, the significance of the observation can be strengthened through use of the Z+H production modes, and also using the $H \to \tau^+\tau^-$ channel discussed in Section 5.3 following.

We have also evaluated the potential of the LHC to make the same measurement, and find that for Higgs masses less than 70 GeV/c^2, the LHC measurement is easier than the Tevatron due to better statistics, but for masses greater than 70 GeV/c^2, the LHC measurement is much more difficult due to larger top backgrounds.

Some more general conclusions about Light Higgs detection at the Tevatron are given in Section 5.5.

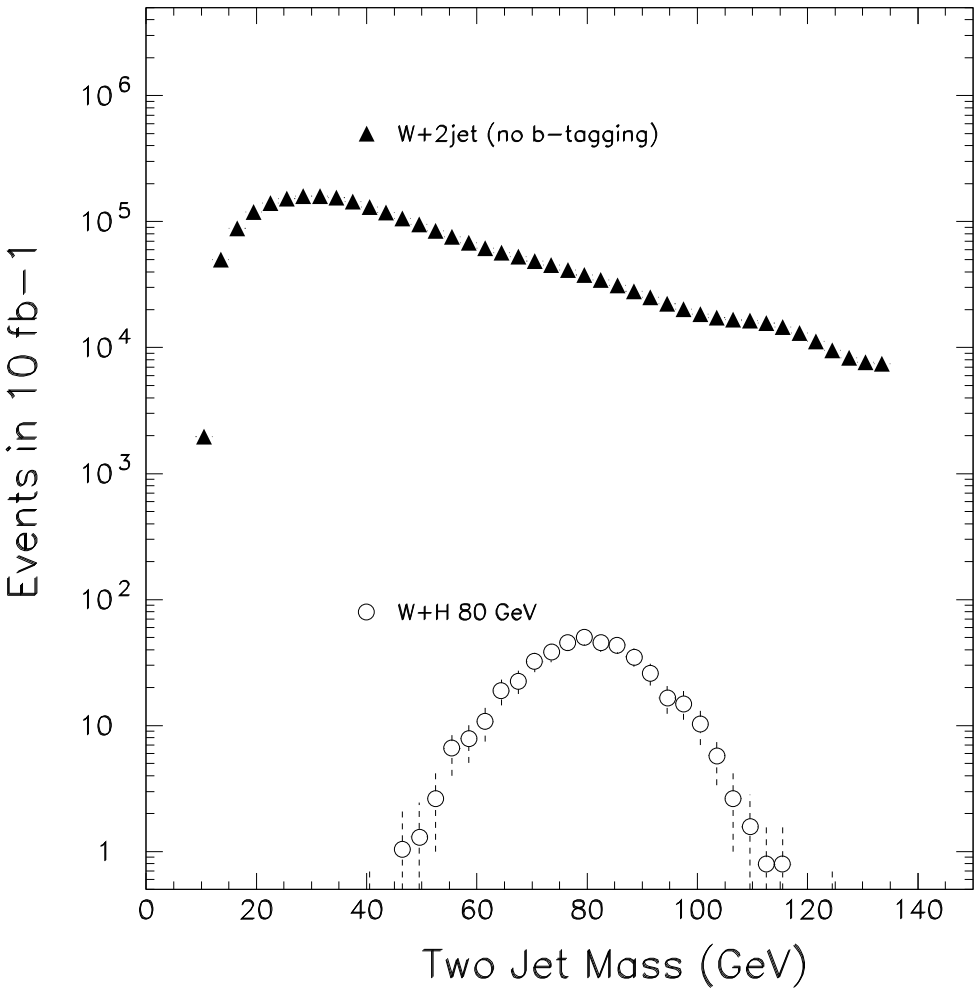

Figure 5.1: The W+2 jet mass distribution measured with CDF data and the expected W+H signal, all before b tagging is applied.

Process	Total σ (fb)	$\sigma\times$BR (fb)	Ref. [3] # Partons in 10 fb^{-1}	This Study # Partons in 10 fb^{-1}	This Study # Jets in 10 fb^{-1}
WH (60 GeV)	1260	230	221	250	166
WZ	3192	110	0	7	7
$W + b\bar{b}$	50607	11246	300	322	564
$t\bar{t}$	6200	1837	8	21	5
W^*	594	132	30	10	9
tqb	2366	526	11	5	15
WH (80 GeV)	575	105	138	120	98
WZ	above	above	83	69	69
$W + bb$	"	"	194	216	270
$t\bar{t}$	"	"	8	33	4
W^*	"	"	44	22	29
tqb	"	"	16	12	12
WH (100 GeV)	289	53	75	60	52
WZ	above	above	102	104	77
$W + bb$	"	"	125	113	134
$t\bar{t}$	"	"	11	30	5
W^*	"	"	55	28	21
tqb	"	"	13	17	12
WH (120 GeV)	155	28	38	33	27
WZ	above	above	8	0	16
$W + bb$	"	"	86	92	77
$t\bar{t}$	"	"	13	38	9
W^*	"	"	58	27	17
tqb	"	"	11	27	11

Table 5.1: Comparison of Stange et al. results and this study's results. The Stange et al. results have been renormalized to a 50% b-tagging efficiency. The bins for all of the signal and background numbers are the same as the Stange paper: 1) 60 GeV Higgs, 48-72 GeV; 2) 80 GeV Higgs, 66-96 GeV; 3) 100 GeV Higgs, 84-117 GeV; 4) 120 GeV Higgs, 102-141 GeV.

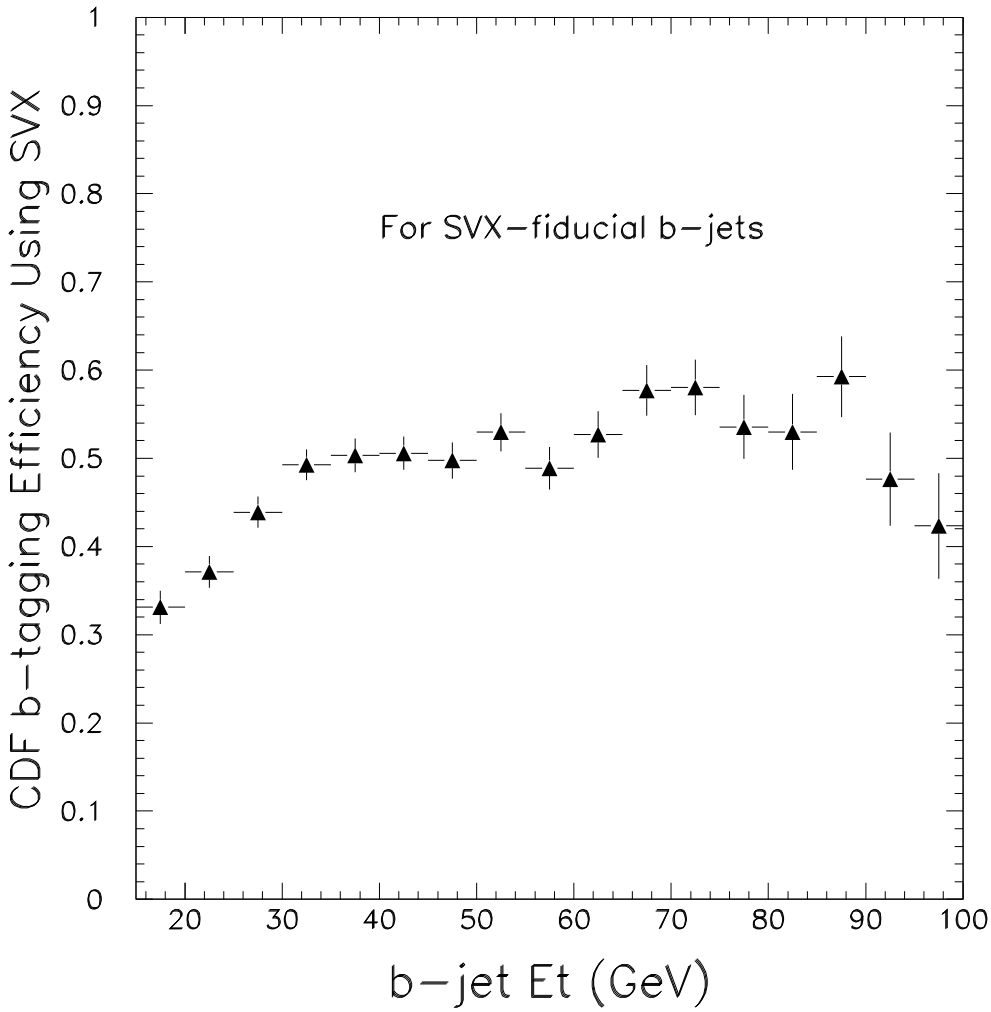

Figure 5.2: The present CDF SVX b tagging efficiency if the b jet centroid is inside the SVX. This represents a reasonable guess for what the b tagging efficiency for the WH process in Tevatron Run II and beyond will be.

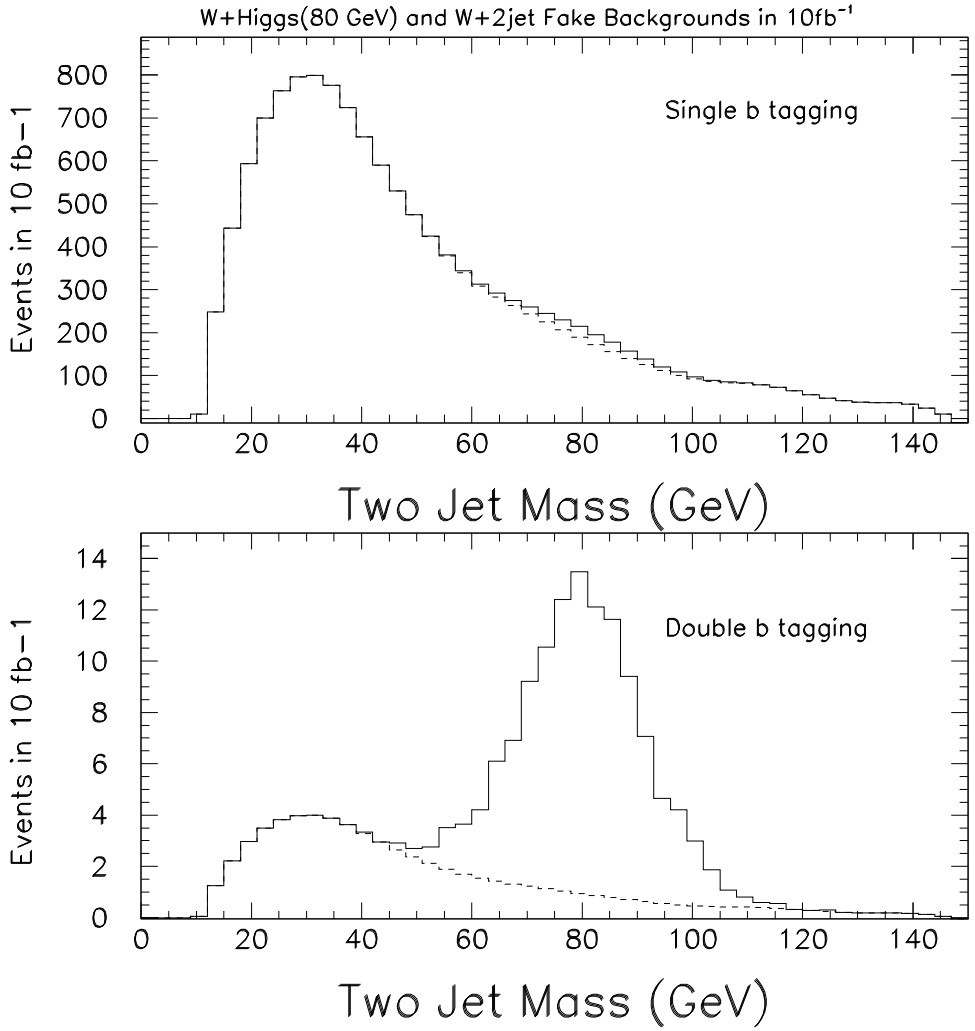

Figure 5.3: The signal+background and background only distributions for single and double b tagging. The background in this case only includes the W+2 jet backgrounds with fake b tag(s).

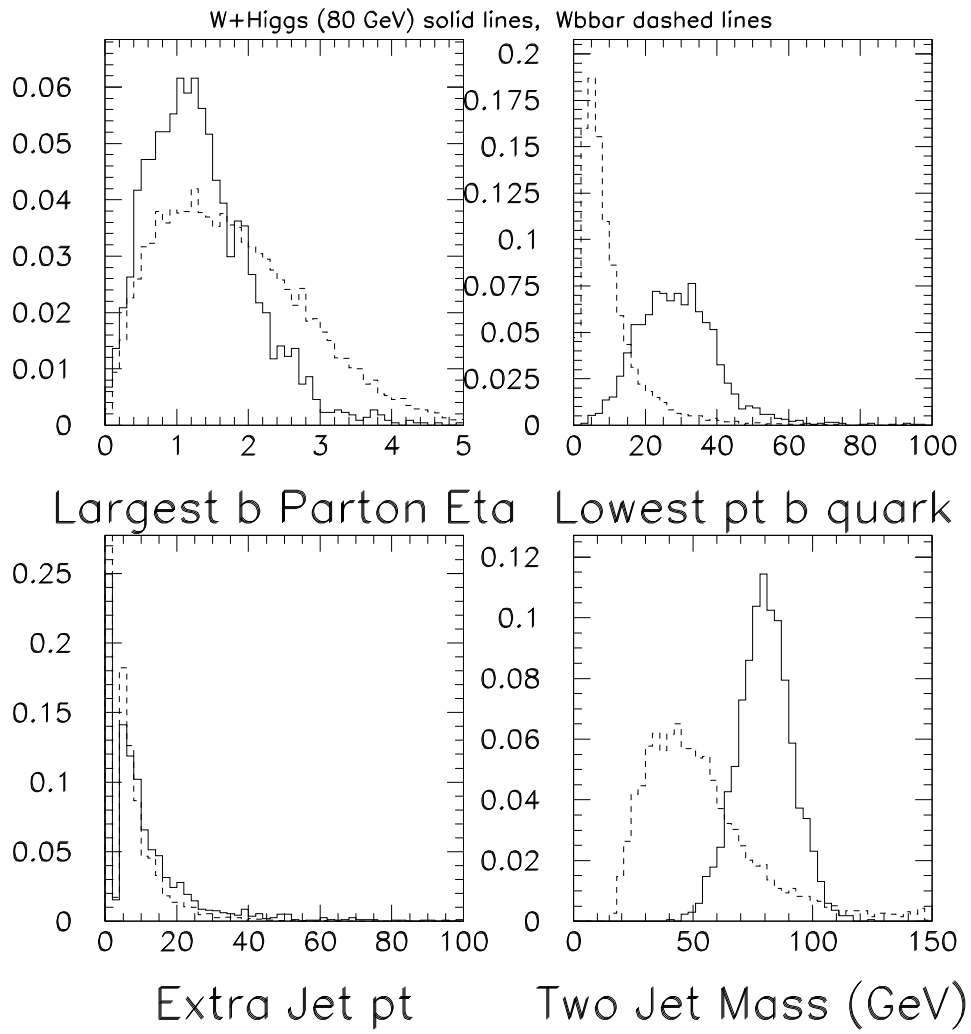

Figure 5.4: Various kinematic properties of the W+Higgs signal (solid) and the $W + b\bar{b}$ backgrounds (dashed). Shown are the largest b parton η, the smallest b parton p_t, the third jet p_t distribution, and the $b\bar{b}$ invariant mass distribution.

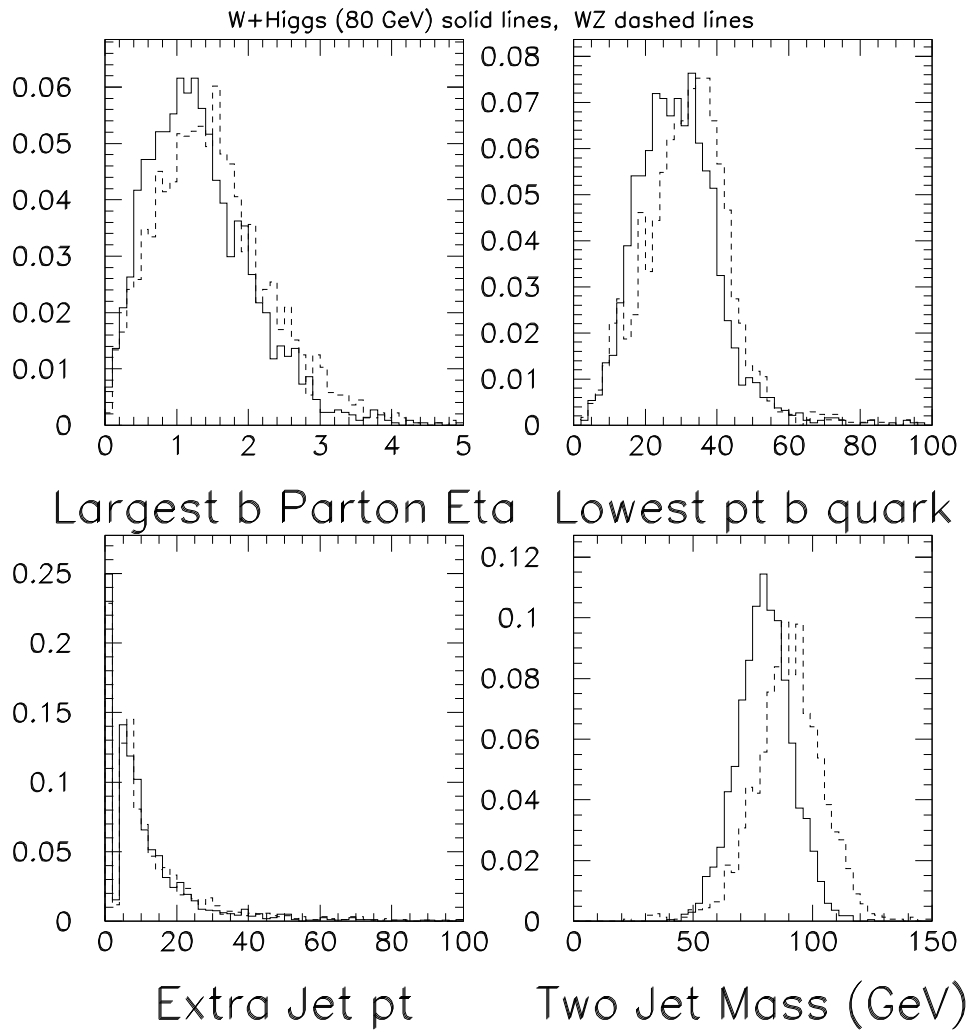

Figure 5.5: Various kinematic properties of the W+Higgs signal (solid) and the WZ backgrounds (dashed). Shown are the largest b parton η, the smallest b parton p_t, the third jet p_t distribution, and the $b\bar{b}$ invariant mass distribution.

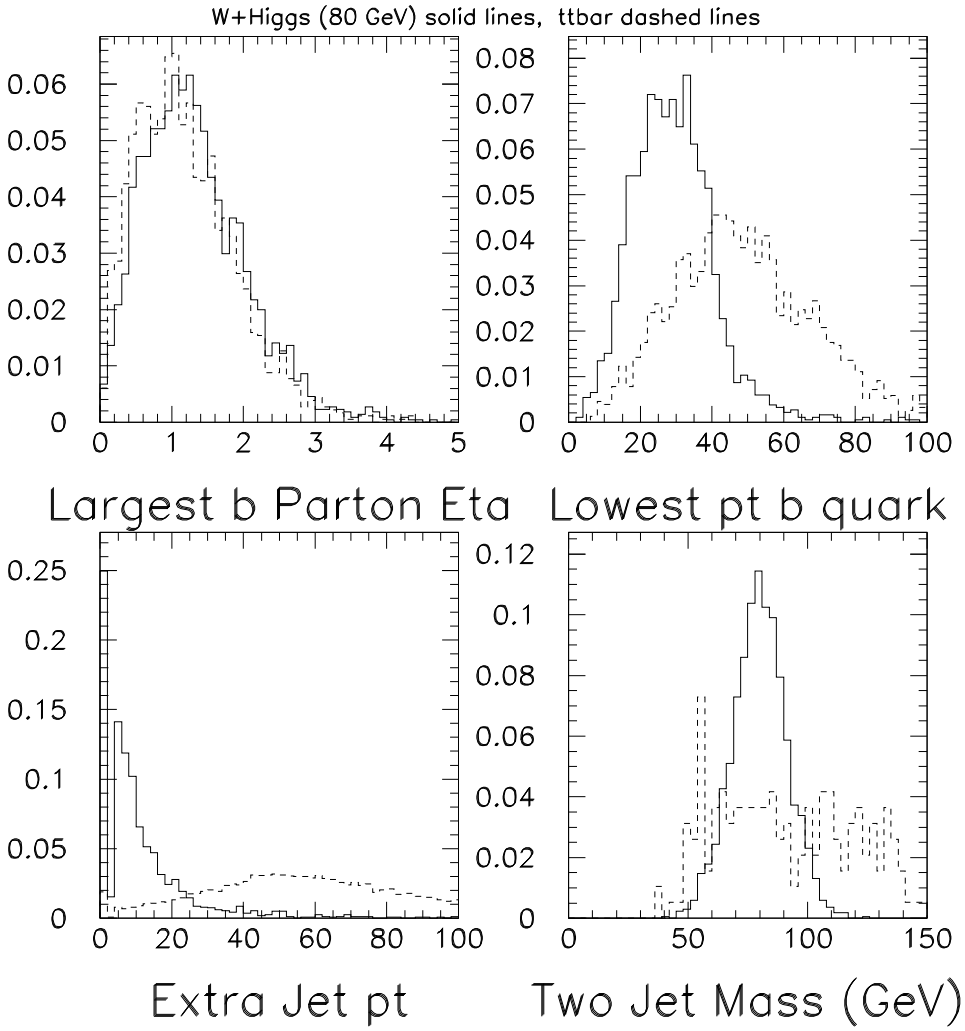

Figure 5.6: Various kinematic properties of the W+Higgs signal (solid) and the $t\bar{t}$ backgrounds (dashed). Shown are the largest b parton η, the smallest b parton p_t, the third jet p_t distribution, and the $b\bar{b}$ invariant mass distribution.

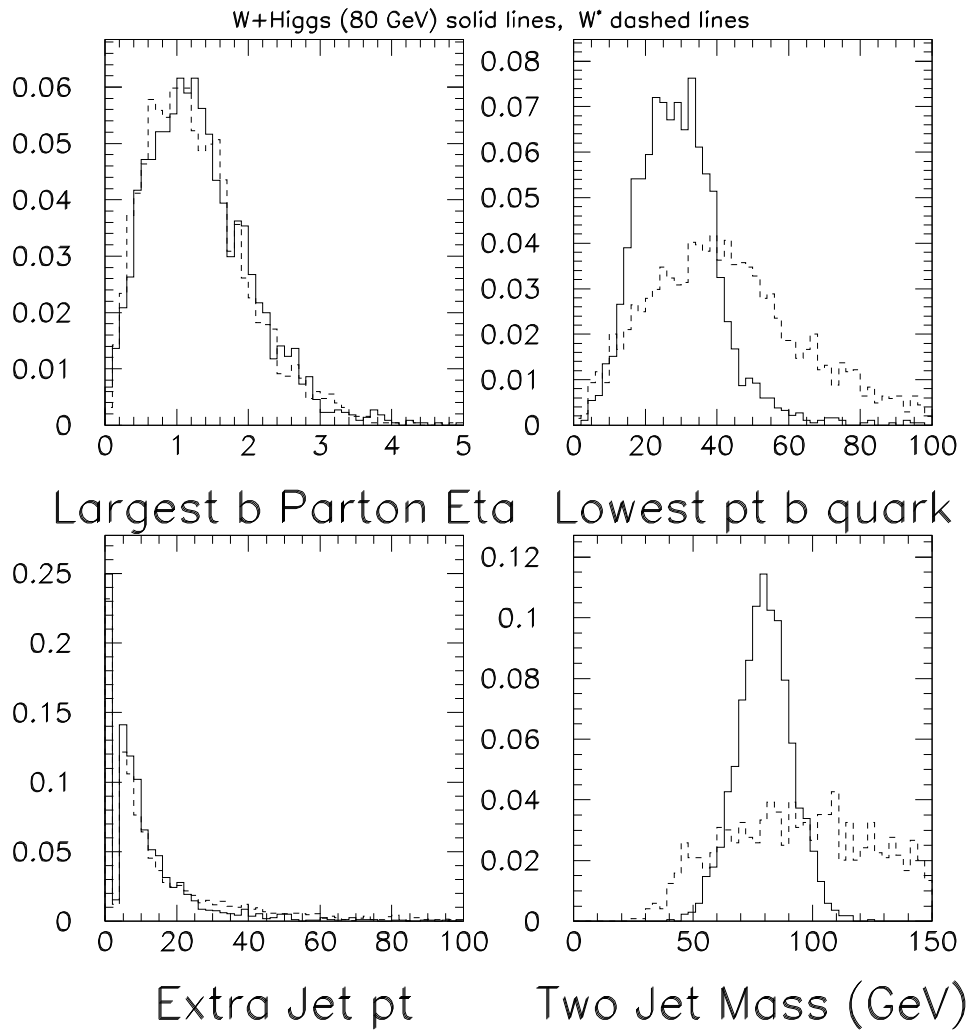

Figure 5.7: Various kinematic properties of the W+Higgs signal (solid) and the W^* backgrounds (dashed). Shown are the largest b parton η, the smallest b parton p_t, the third jet p_t distribution, and the $b\bar{b}$ invariant mass distribution.

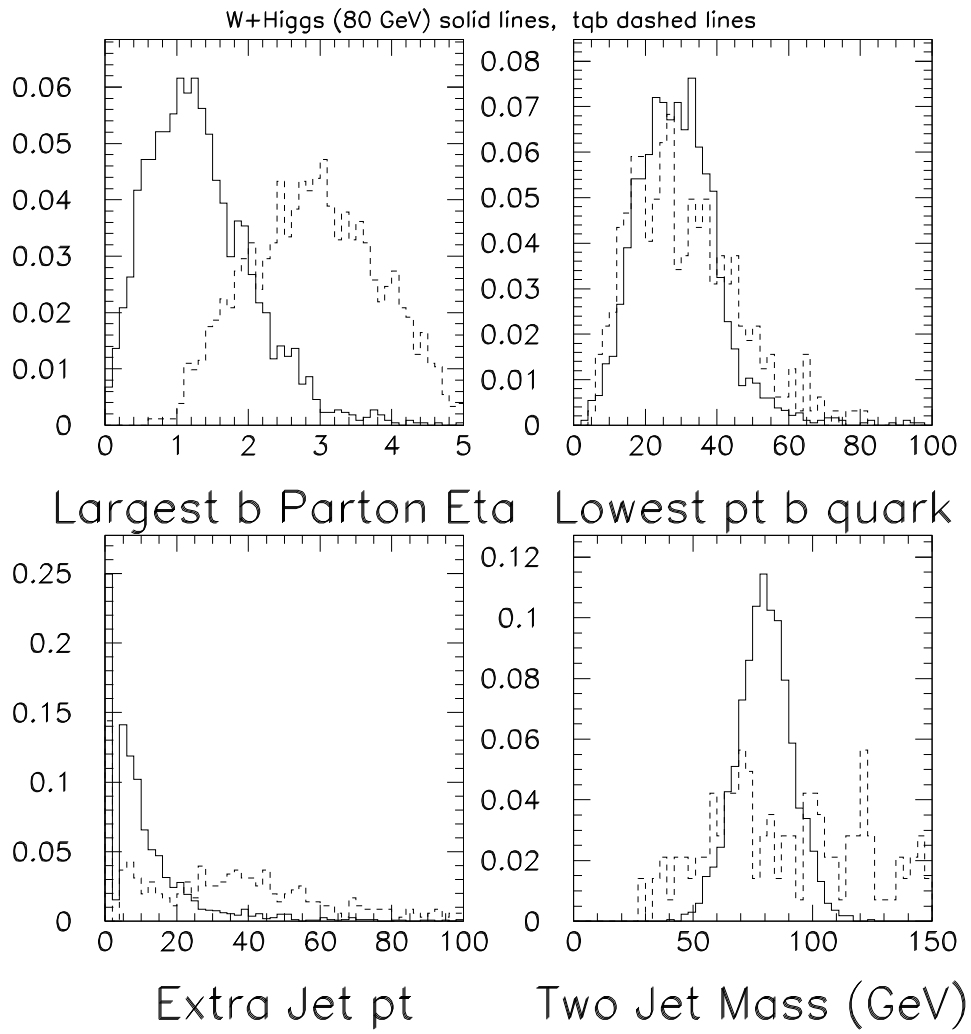

Figure 5.8: Various kinematic properties of the W+Higgs signal (solid) and the tqb backgrounds (dashed). Shown are the largest b parton η, the smallest b parton p_t, the third jet p_t distribution, and the $b\bar{b}$ invariant mass distribution.

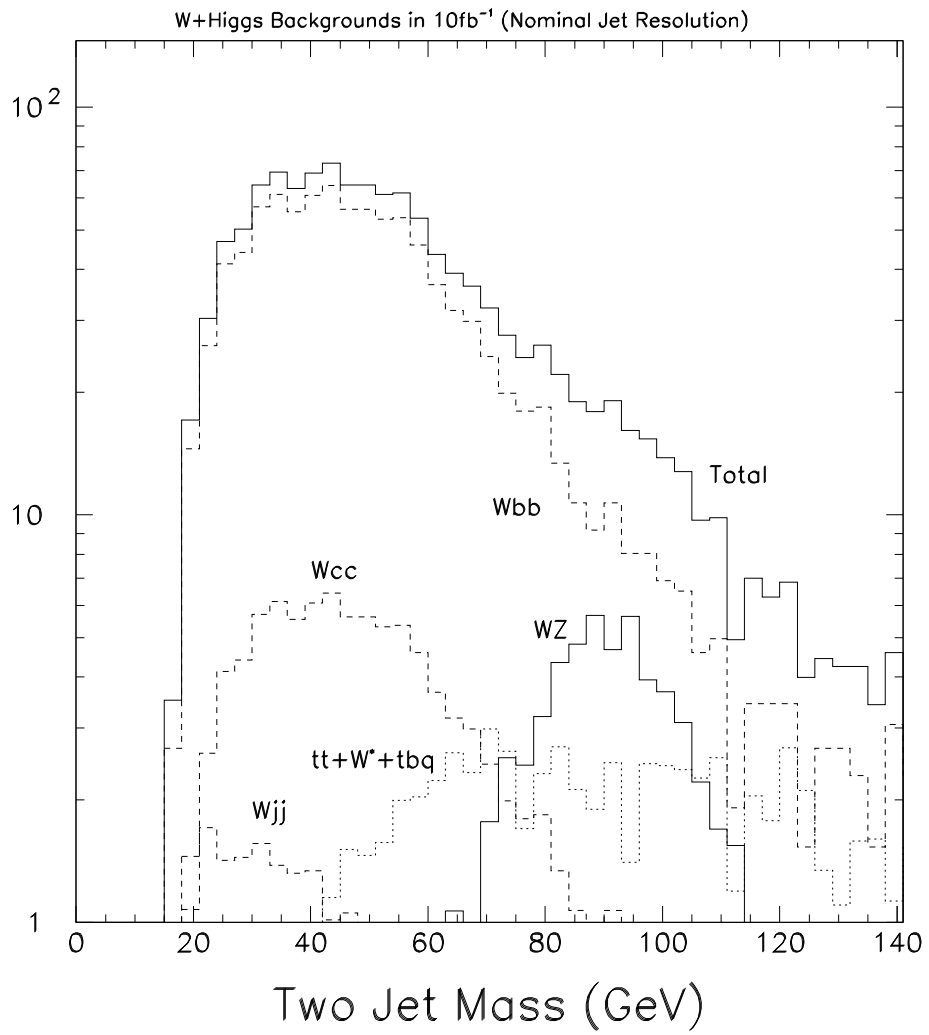

Figure 5.9: The 2 jet mass distributions for the backgrounds to the WH process. Double b-tagging is assumed for each.

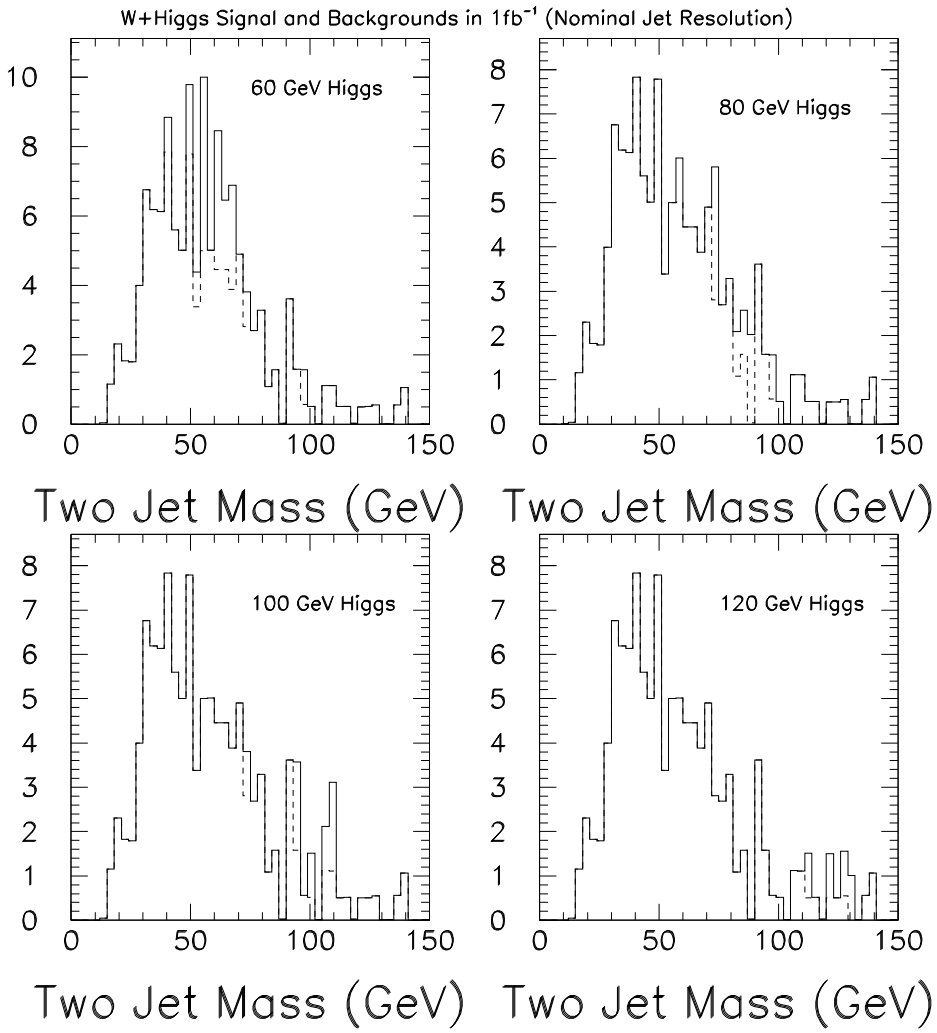

Figure 5.10: The signal+background mass distributions for the WH process with 1 fb^{-1} of data at 2 TeV. The solid line is signal+background, the dashed line the sum of all backgrounds.

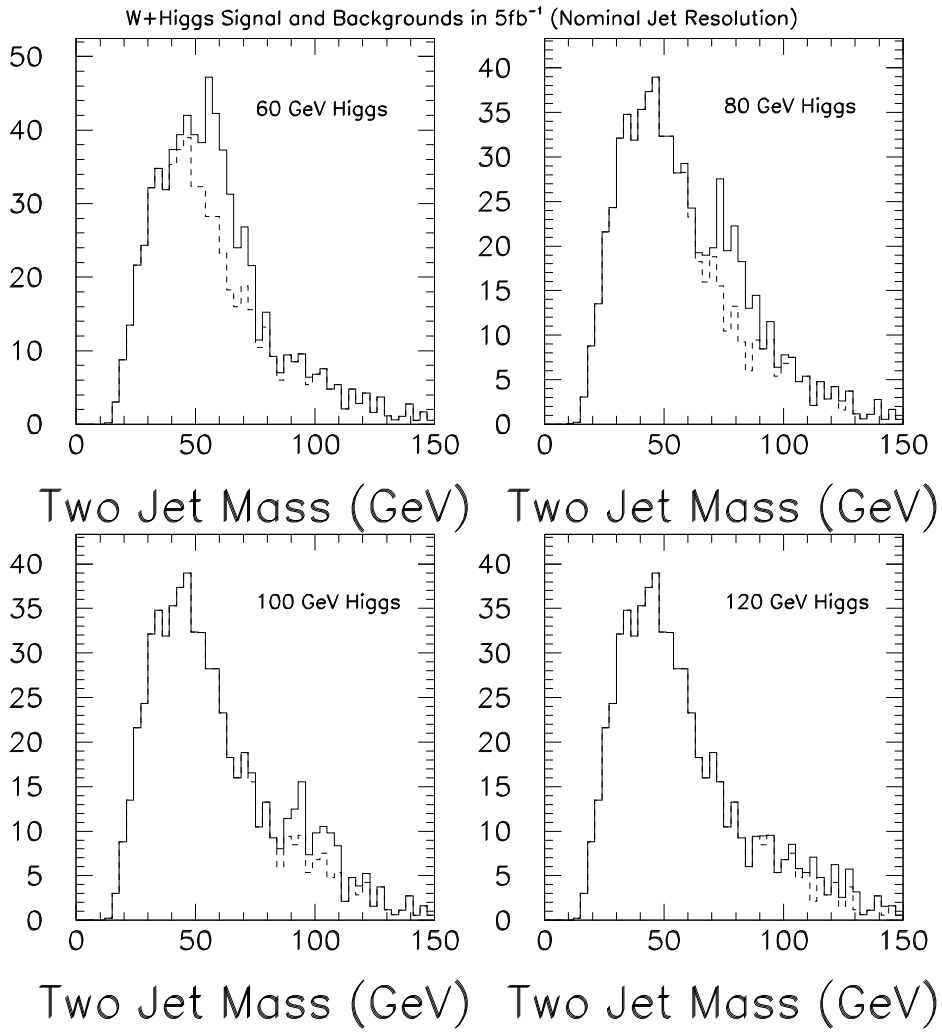

Figure 5.11: The signal+background mass distributions for the WH process with 5 fb^{-1} of data at 2 TeV. The solid line is signal+background, the dashed line the sum of all backgrounds.

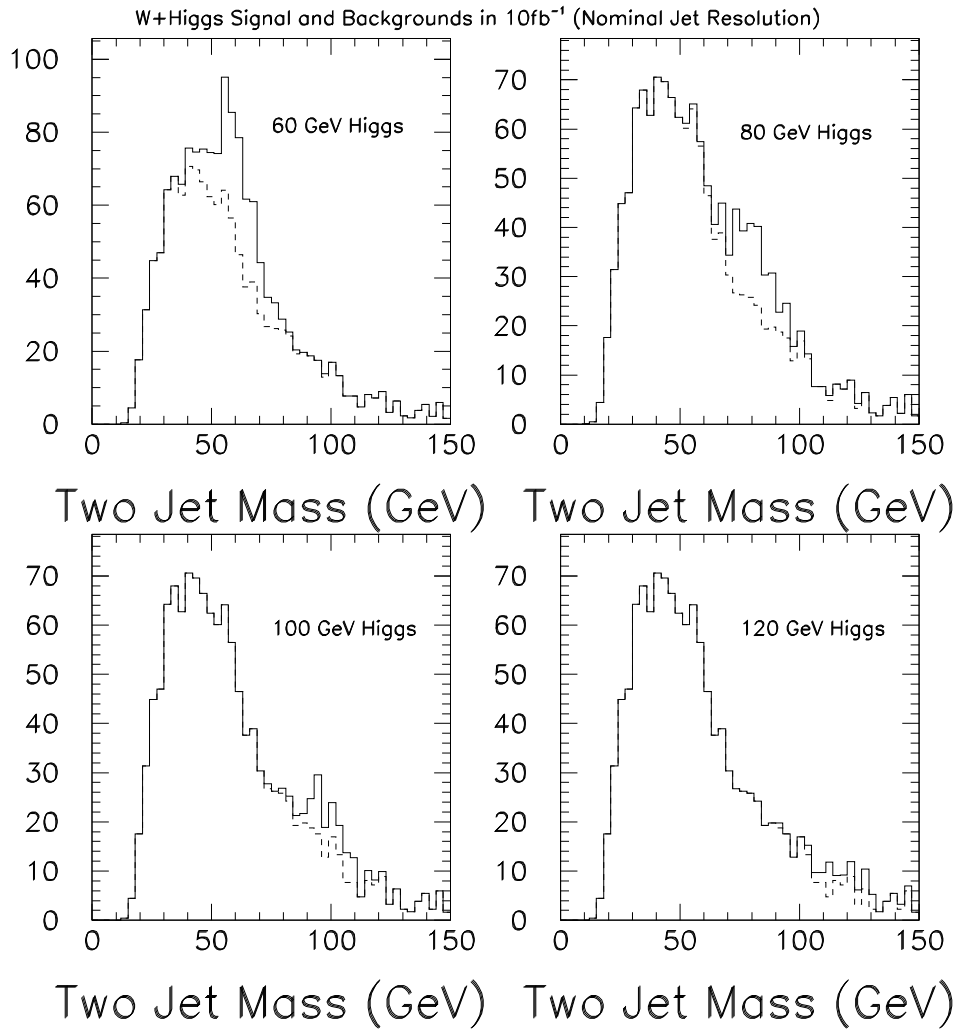

Figure 5.12: The signal+background mass distributions for the WH process with 10 fb^{-1} of data at 2 TeV. The solid line is signal+background, the dashed line the sum of all backgrounds.

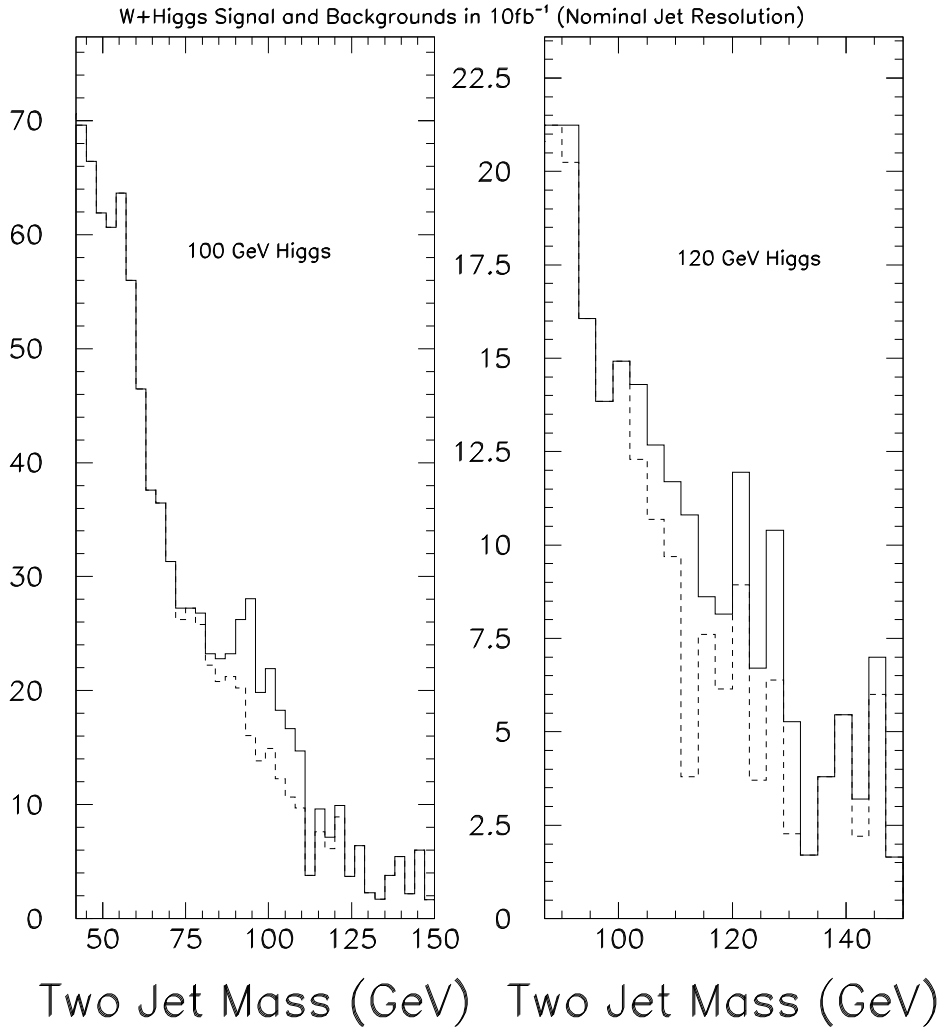

Figure 5.13: Same as the last figure but only the highest two masses.

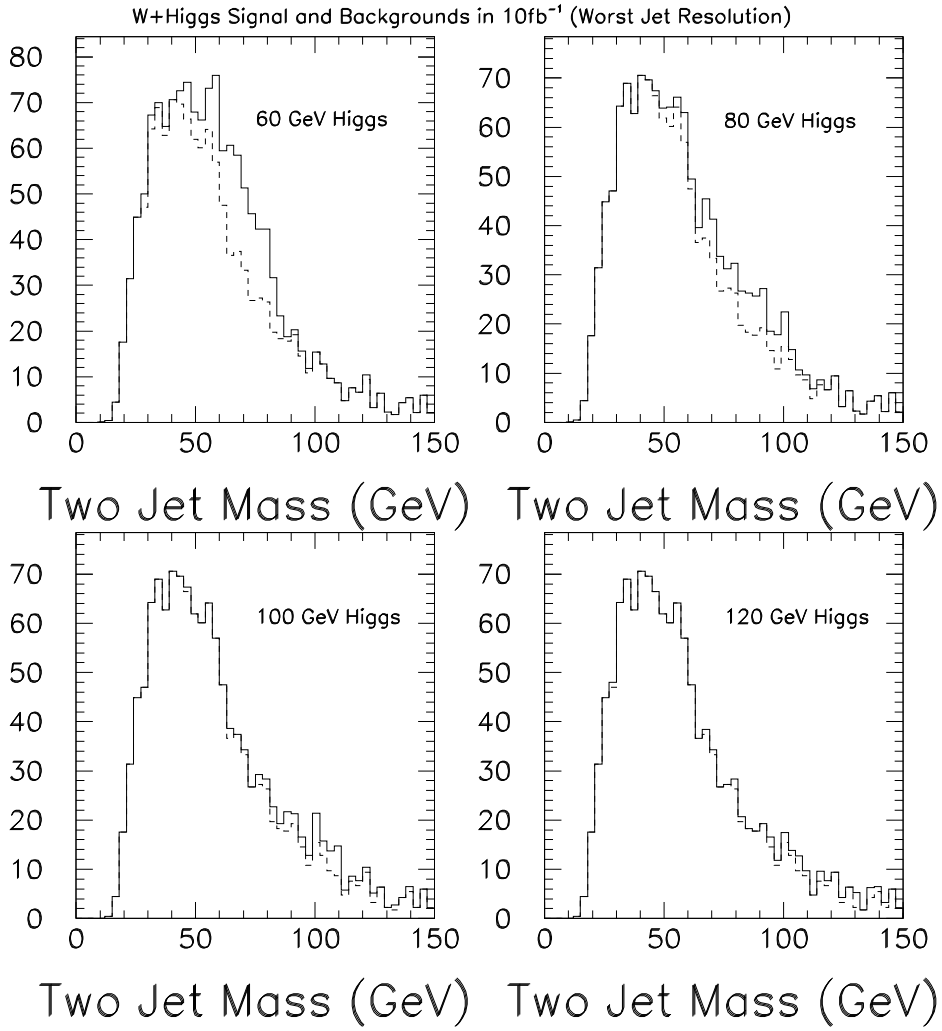

Figure 5.14: The signal+background mass distributions for 10 fb^{-1} of data, but with a worse jet resolution compared to the nominal.

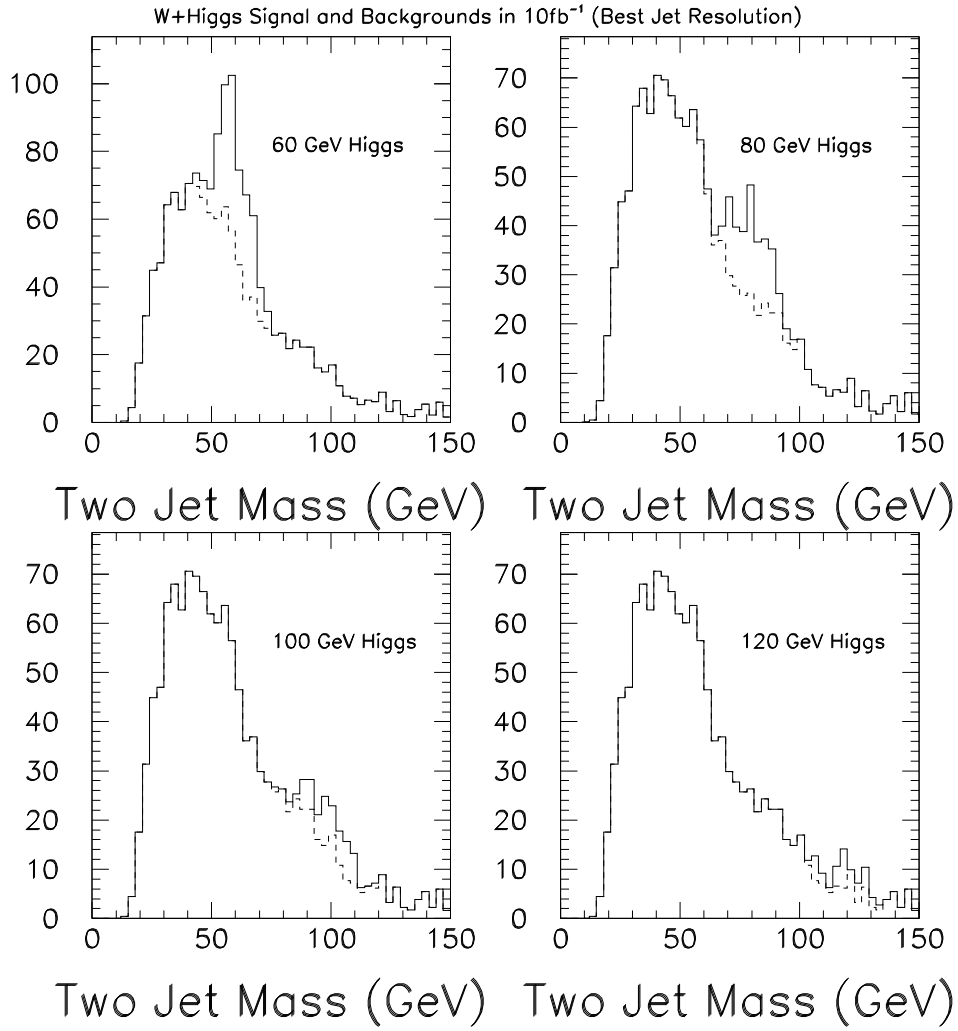

Figure 5.15: The signal+background mass distributions for 10 fb^{-1} of data, but with a better jet resolution compared to the nominal.

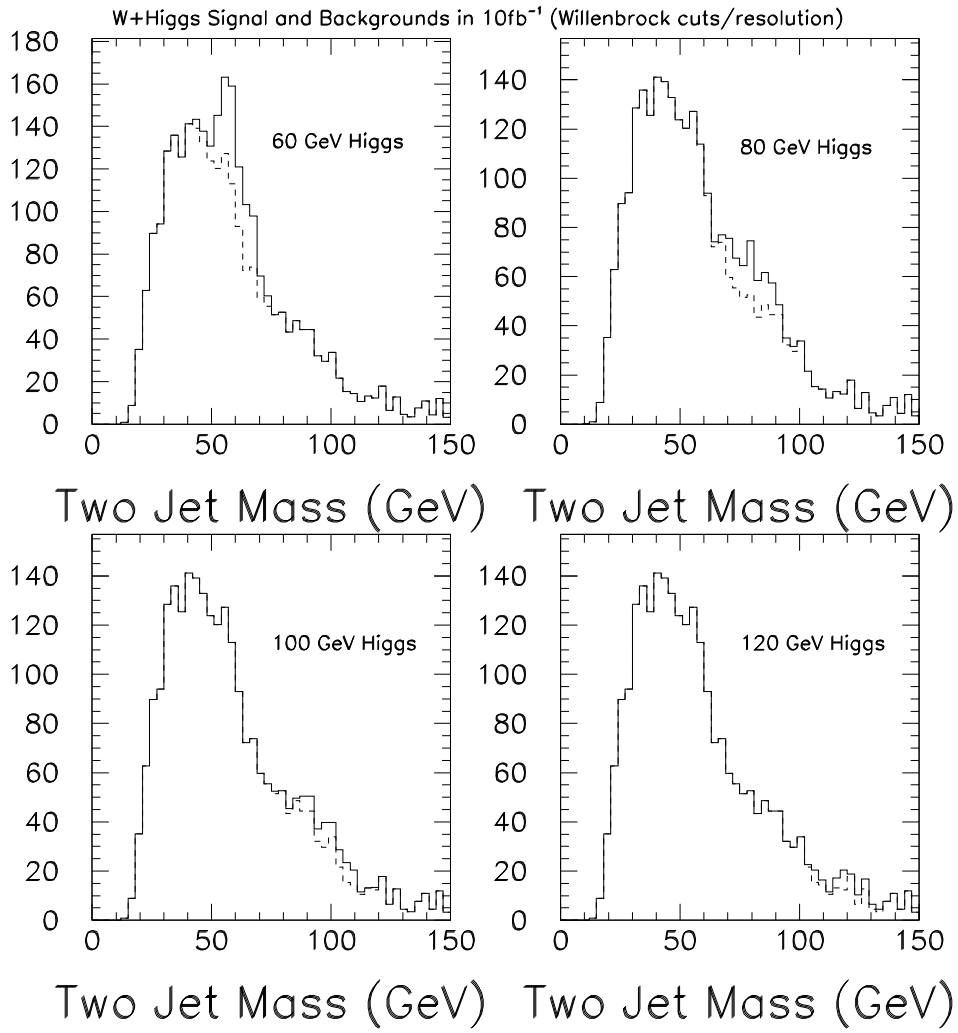

Figure 5.16: The signal+background mass distributions for 10 fb^{-1} of data, using the better jet resolution of the previous plot but removing the effect of optimized cuts.

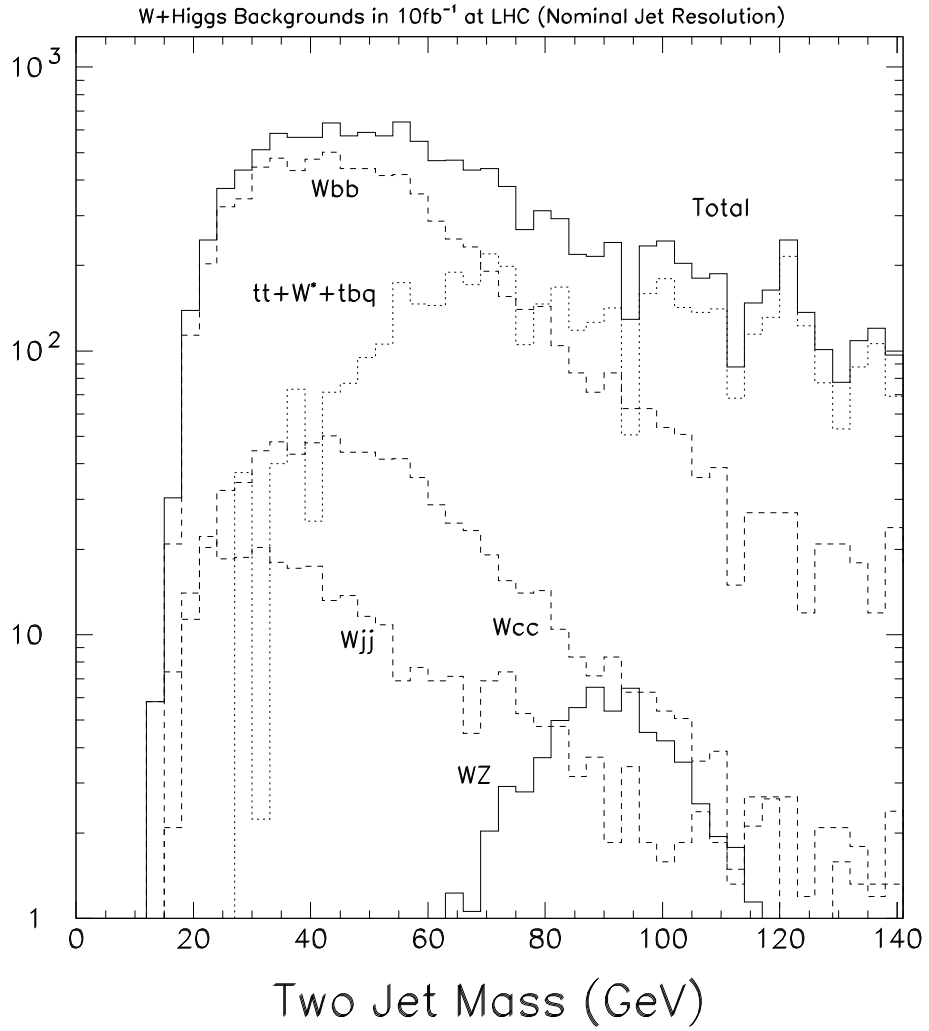

Figure 5.17: The background mass distributions for the WH process with 10 fb^{-1} of data in pp collisions at 14 TeV.

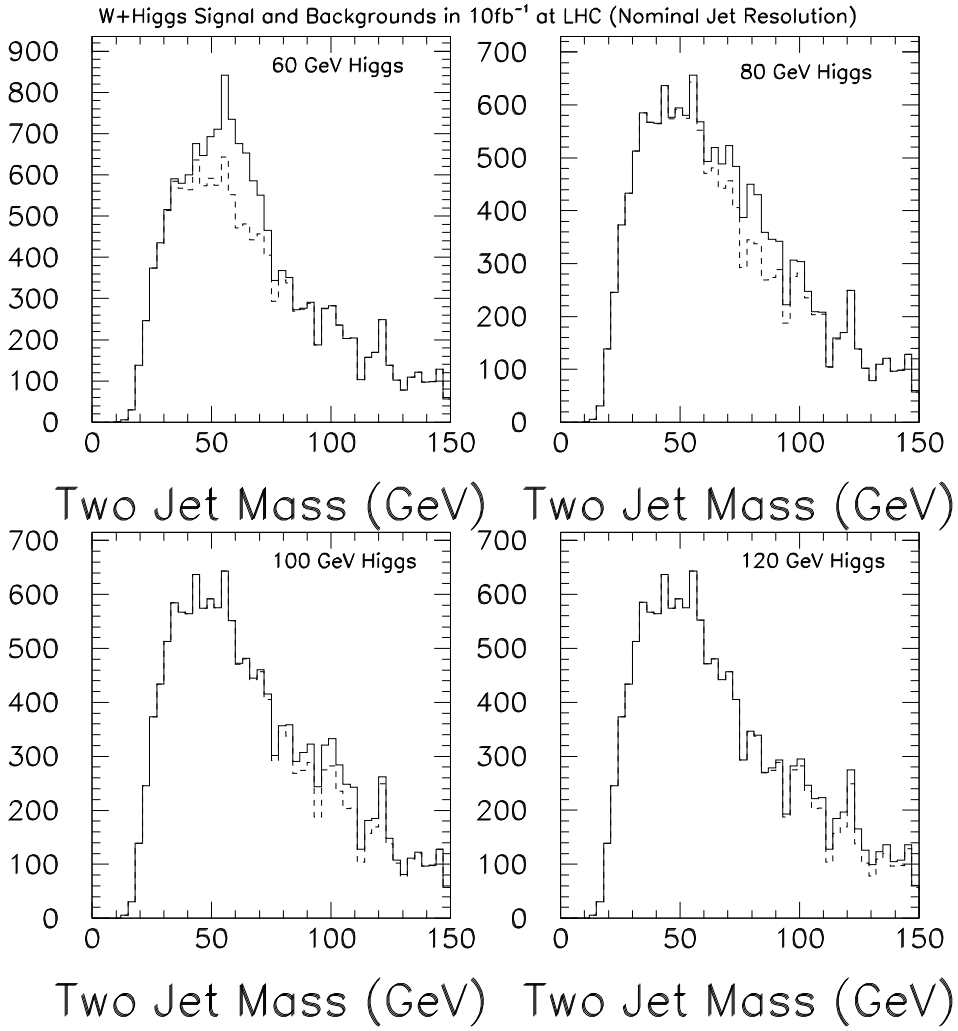

Figure 5.18: The signal+background mass distributions for the WH process with 10 fb^{-1} of data in pp collisions at 14 TeV. The solid line is signal+background, the dashed line the sum of all backgrounds.

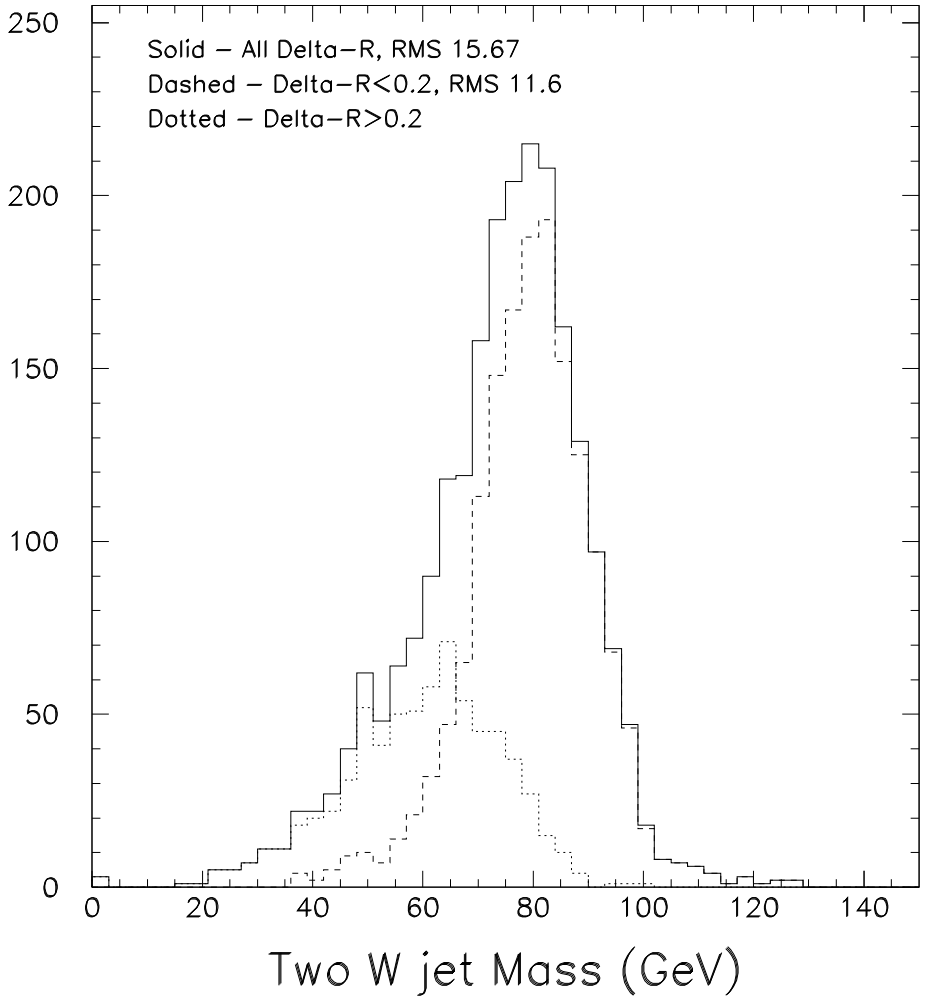

Figure 5.19: The 2 jet mass distribution from a W decay. The solid distribution is for all events, the dashed is for those events when the match between parton and jet is less than 0.2, the dotted is when the match is greater than 0.2.

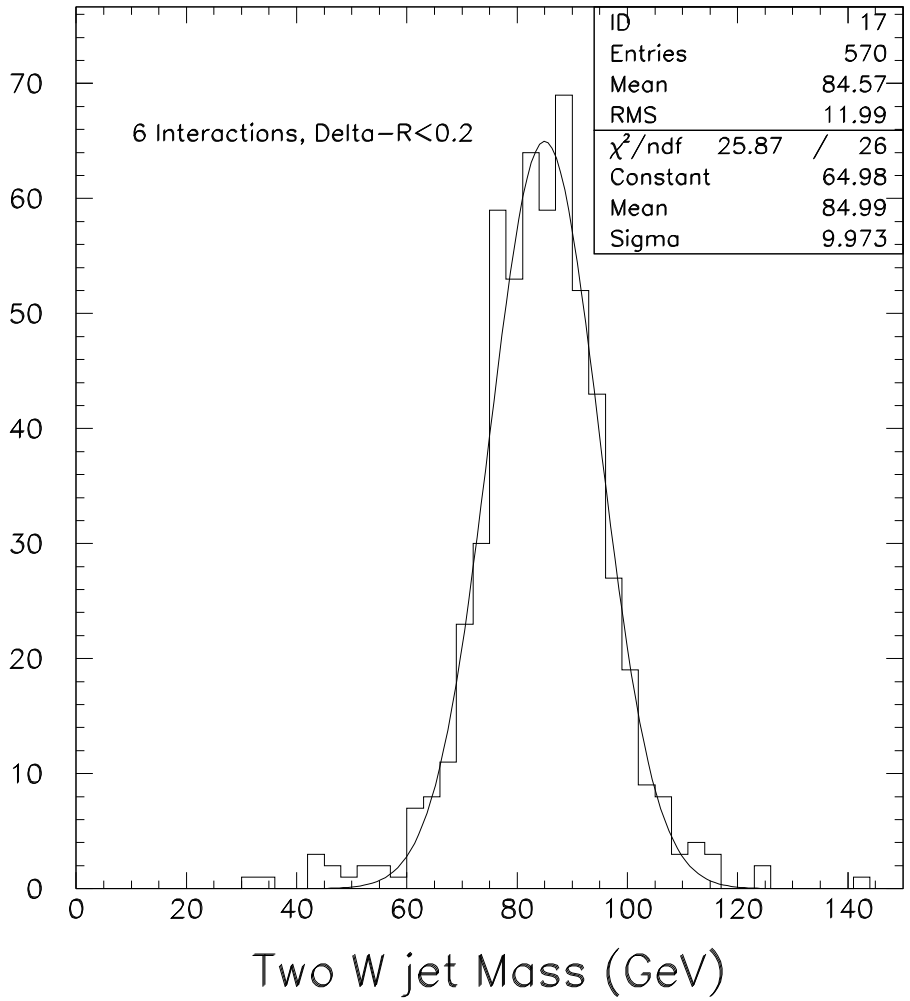

Figure 5.20: The 2 jet mass distribution from a W decay with six interactions.

5.3 $q\bar{q} \to (W,Z)H$ with $H \to \tau^+\tau^-$

The motivation for this work was derived from a paper by S. Mrenna and G. Kane [4], which suggests that all (W,Z)H channels should be combined, and that the $H \to \tau^+\tau^-$ channel adds to the $W + H \to l + \nu + b + \bar{b}$ channels to give good statistical significance for Higgs masses up to 130 GeV/c^2 in a data set over 10 fb^{-1}.

5.3.1 Signal Process

The Higgs is produced in association with an intermediate vector boson in the processes

$$p\overline{p} \to W + H \quad \text{and} \quad p\overline{p} \to Z + H. \tag{5.1}$$

Since not all decay products of the τs are reconstructed we cannot directly reconstruct the Higgs. We follow the technique suggested in reference [4] and reconstruct the $\tau\tau$ mass from the direction of the τs and the transverse momentum of the $\tau\tau$ system, $\vec{p}_T(\tau\tau)$. Let $\hat{\imath}$ and $\hat{\jmath}$ be unit vectors in the plane transverse to the beam in direction of the τs. If they are linearly independent we can solve the equation

$$\vec{p}_T(\tau\tau) = p_T(\tau_1)\hat{\imath} + p_T(\tau_2)\hat{\jmath} \tag{5.2}$$

for the transverse momenta $p_T(\tau_1)$ and $p_T(\tau_2)$ of the τs. Using the known mass and directions of the τs we can then compute the $\tau\tau$ mass.

We shall only use 1-prong τ decays and approximate the direction of the τs by the direction of their charged daughter particle. In order to be able to reconstruct the p_T of the $\tau\tau$ system we select events in which the vector boson decays hadronically, so that we can attribute any transverse momentum imbalance to the neutrinos from the τ decays. We infer the p_T of the $\tau\tau$ system from the measured transverse momentum of the system that recoils against the Higgs, which is given by the sum of the momenta of all detected particles excluding the decay products of the τs.

5.3.2 Background Processes

The dominant background process is

$$p\overline{p} \to Z(\to \tau^+\tau^-) + jj. \tag{5.3}$$

Other sources of events with $\tau\tau$ pairs are

$$p\overline{p} \to W/Z(\to jj) + Z(\to \tau^+\tau^-), \tag{5.4}$$

$$p\overline{p} \to t(\to \tau^+\nu b)\overline{t}(\to \tau^-\overline{\nu}\overline{b}). \tag{5.5}$$

These are much smaller than the dominant process and we shall neglect them. We did not consider backgrounds due to fake τs, such as

$$p\overline{p} \to W(\to \tau\nu) + j(\to \text{ fake } \tau) + jj. \tag{5.6}$$

5.3.3 Detector Requirements

The detector must be capable of measuring transverse momentum balance ($\not{p}_T$) with excellent resolution. We assume that the detector can identify jets with $|\eta| < 3$ and measure their energy E with a resolution of $\sigma_E = 0.8\sqrt{E} \oplus 0.03E$.

We shall in the following assume that we can identify 1-prong τ decays with 100 % efficiency if the charged daughter particle is within $|\eta| < 3$ and has $p_T > 5$ GeV. This is obviously not realistic, but the quoted yields can easily be scaled by the τ detection efficiency for a given detector.

This requires a hermetic and uniform calorimeter with good energy resolution and a good tracking system that extends into the forward regions. A vertex detector might be of use in detecting the τ decay vertex.

5.3.4 Signal and Background Yields

To enhance the signal process against the dominant Z background we make the following cuts:

- transverse momentum of $\tau^+\tau^-$ pair $p_T(\tau\tau) > 20$ GeV,
- two jets with $p_T > 15$ GeV and $60 < m(jj) < 110$ GeV,
- $\not{p}_T > 40$ GeV,
- $p_T > 5$ GeV for charged particles from τ decays,
- opening angle between τs $|\Delta\phi(\tau\tau) - \pi| > 0.6$.

We use PYTHIA to simulate the signal and background processes but estimate the rejection power of the jet cuts for the Z background from data taken by DØ. The following table lists event yields for $m_H = 120$ GeV and 100 fb^{-1}. The column σB gives the production cross section times all branching ratios, including the branching ratios of the τs to 1-prong final states. We use $B(H \to \tau\tau) = 8\%$ [9]. The next column gives the total number of events expected after all selection cuts and the last column lists the number of events expected with $105 < m(\tau\tau) < 129$ GeV.

process	total σ	σB	yield after cuts	$m(\tau\tau)$ cut
$H + W/Z$	230 fb	9.4 fb	157	107
$Z + jj$	6.5 nb	180 pb	8030	940

5.3.5 $\tau\tau$ Mass Resolution

The $\tau\tau$ mass resolution is crucial in distinguishing a Higgs signal from the Z background. We studied the effect of various detector resolutions on the $\tau\tau$ mass resolution. Figure 5.21

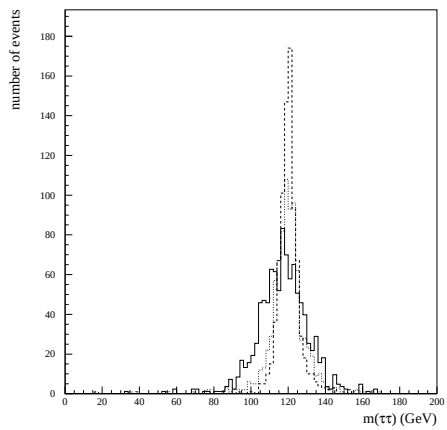

Figure 5.21: Reconstructed $\tau\tau$ mass distribution for $m_H = 120$ GeV with different resolution effects

shows the reconstructed $\tau\tau$ mass distribution for $m_H = 120$ GeV. The true $\tau\tau$ mass distribution is a delta function at 120 GeV. The dashed histogram shows the effect of approximating the τ directions by the directions of their charged daughter particles. The dotted histogram includes in addition a gaussian smearing of the x and y components of the $\not{p}_T$ vector independently by 3 GeV. This is representative of the $\not{p}_T$ resolution observed by DØ for minimum bias events, due to particles lost down the beam pipe and the calorimeter resolution. The solid histogram finally also includes the effect of the jet energy resolution in the calorimeter.

The $\tau\tau$ mass distributions can be fit well with two gaussians of different widths but equal mean. Figure 5.22 shows this for $Z \to \tau\tau$ decays (solid points) and $H \to \tau\tau$ decays (open points). The mass resolution is about 10 GeV with substantial nongaussian tails. For a 120 GeV Higgs ≈68% of the events have $105 < m(\tau\tau) < 129$ GeV and ≈95% of the events have $89 < m(\tau\tau) < 145$ GeV.

5.3.6 Significance of Signal

Figure 5.23 and Figure 5.24 show the $H \to \tau\tau$ signal for $m_H = 120$ GeV superimposed on the $Z \to \tau\tau$ background for a data sample of 100 fb^{-1}. The dashed line shows the Higgs signal, the solid line shows background only and the data points show signal+background. The error bars indicate the expected statistical fluctuations for 100 fb^{-1}. The event yield within $\pm 1\sigma$ of m_H suggests that we should expect a signal with about 3.5 standard deviations significance. However, to achieve this significance exact *a priori* knowledge of the Z background is required.

This result differs somewhat from reference [4]. The difference is largely due to different assumptions about the $\not{p}_T$ resolution. This study assumes the resolution achieved in existing detectors while reference [4] assumed an improved resolution in the upgraded detectors.

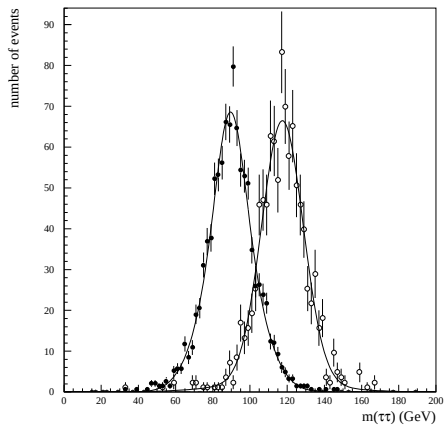

Figure 5.22: Reconstructed $\tau\tau$ mass distribution for $m_H = 120$ GeV and $Z \to \tau\tau$ decays

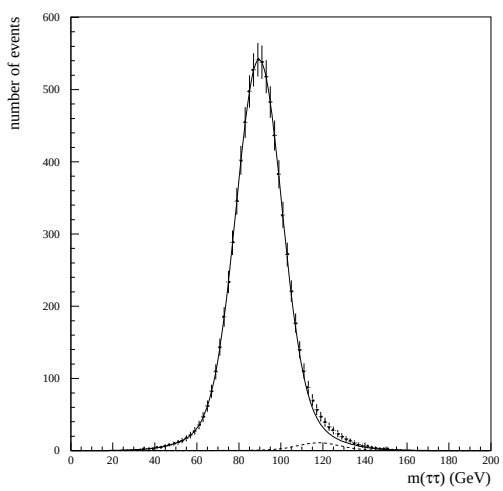

Figure 5.23: Expected $Z \to \tau\tau$ background and $H \to \tau\tau$ signal.

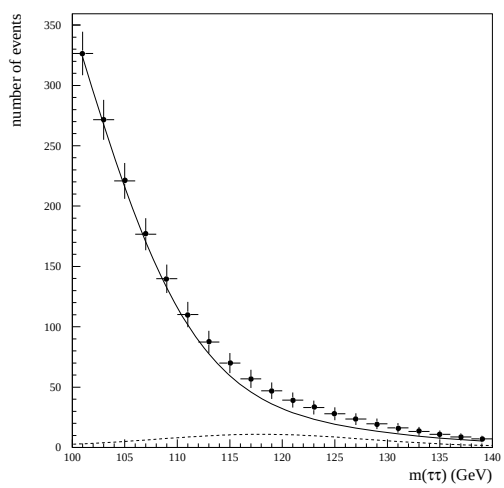

Figure 5.24: Enlarged region of previous figure.

5.3.7 Conclusions on $H \to \tau\tau$ Mode

It seems doubtful that we can establish the existence of the Higgs boson in this channel alone against the $Z \to \tau\tau$ background. However this channel may be combined with results from the $H \to b\bar{b}$ channel to confirm a signal and to increase its statistical significance. It will also constrain the $H \to \tau\tau$ branching ratio relative to $H \to b\bar{b}$ which should be consistent with that expected for Higgs decay.

5.4 Other Accelerators

5.4.1 LEPII

As described in the Introduction, the reach in Higgs mass of LEP II depends on the machine energy, roughly $m_H < \sqrt{s} - M_Z - (5-10)$ GeV. The current plan is for $\sqrt{s} = 184$ GeV, which covers up to $m_H < 85$ GeV, and in 1998 the energy will be increased to 192 GeV, which covers up to $m_H \approx 95$ GeV.

It is technically possible to increase the energy to $\sqrt{s} = 205$ GeV by nearly doubling the number of superconducting cavities over the current plan. This would cover up to $m_H < 105$ GeV. It is conceivable that an energy as high as $\sqrt{s} = 240$ GeV could be attained with yet more superconducting cavities and a cryogenics upgrade. This would cover up to $m_H < 140$ GeV, and would thus cover the entire light intermediate-mass Higgs region. There is no consideration of either of these energies at present, since they are incompatible with the approved LHC construction.

5.4.2 LHC

As described in the introduction, the light intermediate-mass Higgs region is difficult at the LHC. The main hope is the rare decay mode $H \to \gamma\gamma$. The dominant decay mode $H \to b\bar{b}$ may be accessible via $q\bar{q} \to WH$ [3, 4, 6, 7] (the same process as at the Tevatron) and $gg \to t\bar{t}H$ [8]. The ATLAS Collaboration has investigated both of these processes [2]. Their results are encouraging, but neither of these modes can be considered as established at the LHC at this time. Both suffer from enormous top-quark backgrounds, which are much less problematic at the Tevatron.

5.4.3 NLC

Higgs discovery is straightforward at a higher-energy e^+e^- collider, such as the NLC, via $e^+e^- \to ZH$, the same as at LEP II. The reach in Higgs mass is limited only by machine energy, roughly $m_H < \sqrt{s} - M_Z - 10$ GeV. To cover the light intermediate-mass region, $m_H = 80 - 130$ GeV, requires a machine of energy $\sqrt{s} > 230$ GeV. This energy could potentially be attained at LEP II, as described above.

5.5 Conclusions

The mass of the Higgs boson is a free parameter in the standard model of electroweak symmetry breaking. We must therefore be prepared to cover the range of masses from 65 GeV up to about 1 TeV. Precision electroweak experiments suggest that the Higgs-boson mass may lie at the lower end of this range. Furthermore, in the minimal supersymmetric Higgs model, the lightest Higgs boson is less massive than about 125 GeV. Thus there are good reasons to be concerned with the "intermediate mass" region, 65 GeV $< m_H <$ 130 GeV.

We have found promising sensitivity for the discovery of an intermediate-mass Higgs boson at the Tevatron via the process $q\bar{q} \to WH$, with $H \to b\bar{b}$. We tentatively conclude that a Higgs mass of 80 GeV can be reached with about 5 fb^{-1}, a mass of 100 GeV with about 10 fb^{-1}, and a mass of 120 GeV with about 25 fb^{-1}. These results are very encouraging, and suggest that the Tevatron could play a significant role in the quest for an intermediate-mass Higgs boson.

Our analysis makes use of three plausible assumptions, for which there is some support, but which have yet to be established, and represent important areas in need of further research. The first is that the signal-to-background ratio can be improved, by about a factor of two, by a judicious choice of cuts (suggested in Ref. [7]), without a significant loss in signal rate. The second is that the $b\bar{b}$ invariant-mass resolution can be substantially improved with respect to its present value. Our study indicates that it is important to develop an algorithm to merge gluons radiated from the b quarks back into the reconstructed $b\bar{b}$ invariant mass. The third is that the top-quark backgrounds, which become significant for masses above 100 GeV, are indeed manageable. The issues involved in the last two assumptions are, in fact, an extension of the top-quark physics program.

Some other pertinent considerations are as follows:

- The WH with $H \to b\bar{b}$ process also has some potential at the LHC. However, we have found that the top-quark backgrounds are relatively much more severe at the LHC, and as a result this process has more promise at the Tevatron.

- The process $q\bar{q} \to ZH$, with $H \to b\bar{b}$ and $Z \to \nu\bar{\nu}$, has not been studied, but has significant potential as a Higgs discovery mode, comparable to that of the WH process. Along with the other issues mentioned above, this is one of the most important areas in need of further research.

- The process $q\bar{q} \to (W,Z)H$, with $H \to \tau^+\tau^-$ and $(W,Z) \to jj$, is difficult at the Tevatron due to the large $(Z \to \tau^+\tau^-)jj$ background, but it may provide confirmation of a signal in the $H \to b\bar{b}$ decay channel. This process is hopeless at the LHC since the background is relatively worse than at the Tevatron.

- If the Higgs boson is discovered at LEP II ($m_H < 95$ GeV), it is potentially accessible at the Tevatron with less than 10 fb^{-1} of integrated luminosity. The Tevatron process, WH, involves the coupling of the Higgs to the W boson, and is therefore complementary to the LEP II process, ZH, which involves the coupling of the Higgs to the Z boson. The ratio of these couplings differs in multi-Higgs models with higher-dimensional

Higgs representations (such as Higgs triplets), so it is a test of the Higgs-doublet structure of the standard model.

- If no Higgs boson is detected at LEP II ($m_H > 95$ GeV), it will be left to future colliders to discover or rule out the Higgs boson. The only established discovery mode for the intermediate-mass Higgs boson at the LHC is the difficult $H \to \gamma\gamma$ mode, which is particularly challenging for $m_H < 100$ GeV. Furthermore, this mode can become invisible for the lightest supersymmetric Higgs boson, which can have enhanced coupling to b quarks. Thus the $H \to b\bar{b}$ decay mode at the Tevatron could be crucial to ensuring that both the standard Higgs boson and the lightest supersymmetric Higgs boson do not escape the gaze of future hadron colliders.

- The intermediate-mass Higgs boson is easily accessible to a very high-energy linear e^+e^- collider of sufficient energy and luminosity via ZH production. As mentioned above, this is complementary to the WH process at the Tevatron.

Our study thus far has been encouraging. Although further study is needed, the opportunity to detect an intermediate-mass Higgs boson at the Tevatron appears promising.

Bibliography

[1] CMS Technical Proposal, CERN/LHCC/94-38, LHCC/P1 (1994).

[2] ATLAS Technical Proposal, CERN/LHCC/94-43, LHCC/P2 (1994).

[3] A. Stange, W. Marciano, and S. Willenbrock, Phys. Rev. D **49**, 1354 (1994); D **50**, 4491 1994 .

[4] S. Mrenna and G. Kane, CALT-68-1938 (1994).

[5] A. Belyaev, E. Boos, and L. Dudko, Mod. Phys. Lett. **A10**, 25 (1995).

[6] D. Froidevaux and E. Richter-Was, Z. Phys. C **67**, 213 (1995).

[7] P. Agrawal, D. Bowser-Chao, and K. Chung, Phys. Rev. D **51**, 6114 (1995).

[8] J. Dai, J. Gunion, and R. Vega, Phys. Rev. Lett. **71**, 2699 (1993).

[9] E. Gross, B. Kniehl, G. Wolf, Z. Phys. C 63, 417 (1994) and erratum Z. Phys. C 66, 321 (1995).